

## Pressure-Induced Crystal-Structure Transition in Fe-Cr Alloys

Amir Broide<sup>1,2,†</sup>, Oleg Rivin<sup>1</sup>, Silvie Maskova<sup>3</sup>, Matthew S. Lucas<sup>4</sup>, Amir Hen<sup>2,5</sup>, Itzhak Orion<sup>2</sup>, Shai Salhov<sup>1</sup>, Michael Shandalov<sup>1</sup>, Antonio F. Moreira Dos Santos<sup>6</sup>, Jamie Molaison<sup>6</sup>, Zhiqiang Chen<sup>7</sup> And Itzhak Halevy<sup>1,2</sup>

<sup>1</sup> Department of Physics, NRCN, Beer-Sheva, Israel

<sup>2</sup> Nuclear Engineering Department, Ben Gurion University - Negev, Beer-Sheva, Israel

<sup>3</sup> Department of Condensed Matter Physics, Faculty of Mathematics and Physics, Charles University, Prague, The Czech Republic

<sup>4</sup> Air Force Research Laboratory, OH, USA

<sup>5</sup> European Synchrotron Radiation Facility (ESRF), Grenoble, France

<sup>6</sup> Spallation Neutron Source (SNS), Oak Ridge National Laboratory, Oak Ridge, TN, USA

<sup>7</sup> National Synchrotron Light Source (NSLS), Brookhaven National Laboratory, NY, USA

Corresponding author: Amir Broide

---

**Abstract:** Elemental Iron undergoes crystal-structure transition from bcc ( $Im\bar{3}m$  space group) to hcp ( $P6_3/mmc$  space group) structure type under the pressure of 13 GPa. With increasing Cr-concentration, the structure transition is shifted to higher pressures (e.g. 18 GPa for  $Fe_{70}Cr_{30}$ ). For Cr-concentrations higher than 47 % we did not see any traces of the phase transition probably because the maximum pressure used (35 GPa) was not high enough to induce the structure transition in the alloys. After releasing the pressure, the cubic symmetry is restored. The Bulk modulus is increasing from 160 GPa (elemental Fe) with increasing Cr concentration up to approx. 30 % Cr. Then it starts to decrease again followed by another increase and subsequent decrease represented by a double-peak dependence on Cr concentration. Hydrogen exposure of  $Fe_{80}Cr_{20}$ , resulting in negligible H absorption to the surface layers, does not bring any significant changes to the crystal-structure properties.

**Keywords:** Crystal structure, Fe-Cr, High pressure, Neutron diffraction, X-ray diffraction

---

Date of Submission: 10-07-2018

Date of acceptance: 24-07-2018

---

### I. Introduction

Chromium ferritic-martensitic steels [1,2] (Cr concentration of 9-12 wt.%) are candidate structural materials for high temperature applications in fusion reactors, Accelerator Driven Systems (ADS) and advanced GEN IV fission reactors [3]. It was shown that the Cr concentration is a key parameter which needs to be optimized in order to guarantee the best corrosion and swelling resistance, together with minimum embrittlement [4]. The temperature dependence of the crystal structure of Fe-Cr alloys was considered to be well known (see fig. 1 for the temperature-composition diagram of these alloys) [5]. However, in recently published papers [6,7] some structural features which are not accounted for by the phase diagram of the Fe-Cr system have been reported. Owing to this fact, the phase diagram of Fe-Cr should be reinvestigated. Fe-Cr alloys are considered for the applications where also the influence of external pressure is very important. Elemental Iron undergoes crystal-structure transition from bcc ( $Im\bar{3}m$  space group) to hcp ( $P6_3/mmc$  space group) structure type under the pressure of 13 GPa [8]. Here we report on the influence of Cr substitution on the structure-transition pressure in Fe-Cr alloys. It is shown that the pressure necessary to induce the structural transition as well as the bulk modulus of these alloys are highly dependent on the Cr-concentration.

### II. Experimental Methods

#### 2.1 Sample Preparation

Several  $Fe_{100-x}Cr_x$  alloys ( $x = 90, 80, 70, 65, 60, 53, 40, 30, 20, 3$ ) were prepared by arc melting stoichiometric amounts of elements (Fe – 99.99% and Cr – 99.995%) under an argon atmosphere. The buttons were turned and re-melted 3-times to ensure homogeneity. The mass loss and surface oxidation after melting were found to be negligible, hence, the samples compositions are expected to be accurate to 0.1 at. %. The samples were cold-rolled to final thickness of 1 mm for X-ray diffraction or cut to long bars with diameter of 1 cm for neutron-diffraction experiments. All samples were sealed into a quartz tube under an argon atmosphere and annealed at 1100 °C for 72 hours with subsequent quenching into ice water. The quenching was performed to prevent the well-known phenomenon called the 475 °C embrittlement, which is related to the decomposition of

the Fe-Cr solid solution to  $\alpha'$ - $\alpha''$  (Fe rich and Cr rich phases) fractions [6,7]. The rapid cooling was used to preserve the high temperature bcc phase.

So as to study the resistance to hydrogen which can significantly influence the integrity of the material, selected samples were subjected to the high H<sub>2</sub> pressure. The samples of cylindrical shape and mass of approx. 0.5g were loaded into a reactor. Then the standard procedure of hydrogenation was performed. So as to remove surface contaminants, the samples were heated to 250 °C in dynamic vacuum (10<sup>-6</sup> mbar) for 2 hours. The reactor was then cooled down and filled with pressurized hydrogen (~120 bar), and the samples were exposed to thermal cycling up to T = 150 °C with subsequent cooling to room temperature with the cooling rate 0.2 °C/min.

The X-Ray diffraction experiments performed on all samples both before and after the annealing were used to confirm the bcc phase. There was no evidence of sigma phase or oxide. EDX (Energy-Dispersive X-ray spectroscopy) measurements on all the samples were carried out to confirm the homogeneity and the compositions of the samples. The absence of phase separation was verified by means of the Scanning Electron Microscopy (SEM).

The samples were stored in oxygen free environment until the X-ray and neutron diffraction measurements were taken. The samples were tested a year later with Angle Dispersive Diffraction (ADS) and no oxidation phase was observed. This diffraction measurements didn't reveal any  $\alpha'$ - $\alpha''$  separation, although it is very difficult to detect the two phases,  $\alpha'$ - $\alpha''$ .

## 2.2 Measurements methods

The high-pressure X-ray diffraction spectra were taken at the X17-C beamline of the National Synchrotron Light Source (NSLS-I) using a "Tel-Aviv" Merrill-Bassett type diamond anvil cell (DAC) [9] in the pressure range of 0 (ambient) to 35 GPa. The sample dimensions for the X-Ray diffraction were ~ 30  $\mu$ m in height and ~ 80  $\mu$ m in diameter. The Be gasket hole (the sample cavity) was ~ 120  $\mu$ m and the diamonds culets were 350  $\mu$ m. The values of these parameters were used to ensure that the data are collected only from the sample.

The pressure in the DAC was measured using the Ruby fluorescence technique [10]. Silicon oil in the sample cavity was used as a pressure medium as well as a non-corrosive environment. The pressure distribution inside the sampling space was checked at different places varying by less than 5%. It is known that the Si oil solidifies at 11 GPa, however, the Van der Waals forces of the solid Si are still hydrostatic and because of that, the pressure distribution is the same at high pressures (less than 5%).

The high-pressure X-ray powder diffraction measurements were taken at discrete pressure steps (about 15 steps) in the pressure range of 0-35 GPa. The data were collected for approximately 15 min for each pressure.

The experiments were conducted in both Energy Dispersive Diffraction (EDS) and Angle Dispersive Diffraction (ADS) configuration of the beam line. The EDS data were collected using the high pure germanium detector at a fixed Bragg angle  $2\theta = 12^\circ$  with the "white beam" energy 20 keV – 100 keV. The ADS experiments were conducted using a monochromatic X-ray beam ( $\lambda = 0.4066 \text{ \AA}$ ) in transmission configuration using the image plate technique. All the EDS and ADS data were converted to Cu-K $\alpha$  radiation wavelength ( $\lambda = 1.5406 \text{ \AA}$ ) for better comparison. The EDS diffraction configuration was mainly used for higher resolution. The disadvantage of this method is the presence of fluorescence lines. The escape peaks were excluded from the Rietveld refinements of obtained patterns. Using this configuration brings also problems with identification of preferred orientation because we can see only very small part of the Debye rings.

The Be-support disk for the diamond (transparent to the X-ray radiation) was used to enable seeing higher d-spacings. The ADS method of diffraction was used to determine the preferred orientation as with this method we receive almost the full Debye rings.

The diffraction patterns were refined using a commercial Rietveld analysis software package [11].

The high pressure neutron diffraction experiments were carried out at the Spallation Neutrons and Pressure (SNAP) diffractometer, located at the Spallation Neutron Source (SNS) at the Oak Ridge National Laboratory (Tennessee, USA) [12]. Neutron diffraction (ND) experiments were performed under external pressure (0 - 27.5 GPa) using a Paris-Edinburgh type anvil cell. The incident neutron beam energy of 25 meV was selected using mechanical chopping. This incident energy was selected to ensure sufficient number of angularly resolved Bragg reflections (~ 6) within the instrumental angular resolution. Also for this energy, most reflections are well separated from the instrumental reflections generated by the anvil. For each measurement, a ~ 0.5 g pellet samples were loaded into the Paris-Edinburgh type anvil cell. No sample holder and no hydrostatic medium were used in this experimental set-up. The ND analysis was performed using the standard Rietveld analysis software package [13].

### III. Results and Discussion

#### 2.1 Crystal structure and composition

EDX measurements verified the homogeneity and the compositions of the samples. X-Ray diffraction experiments performed both before and after the annealing confirmed the bcc phase. The XRD patterns were refined using cubic lattice symmetry (Im-3m space group). The Fe and Cr ions occupy the 2a site. There was no evidence of sigma phase or oxide. The unit-cell parameter is slightly increasing with increasing Cr-concentration (fig. 2).

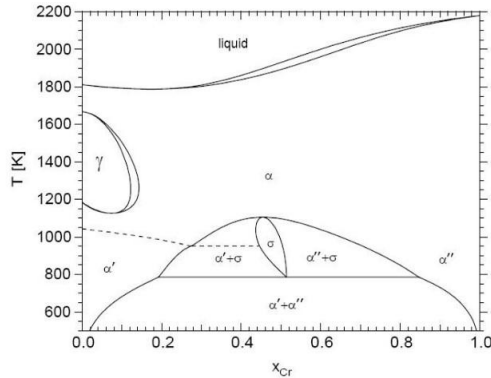


**Figure 1.** The temperature-concentration phase diagram of the Fe-Cr.

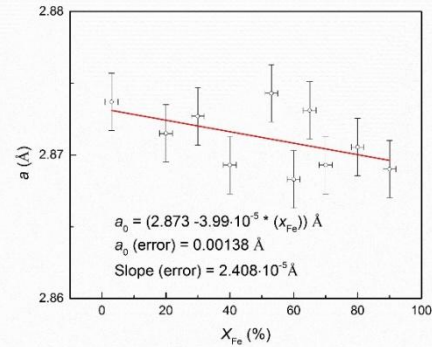


**Figure 2.** The concentration dependence of the unit-cell parameter of Fe-Cr alloys at ambient pressure.

#### 2.2 Hydrogen Absorption

We did not observe any significant pressure drop indicating hydrogen absorption when subjecting the samples to the high H<sub>2</sub> pressure. So as to find the amount of the hydrogen absorbed we have performed controlled temperature-induced desorption in a calibrated evacuated volume (fig. 3), using the constant heating rate 2 K/min. As the release was small we undertook a run with empty reactor from which we obtained release of approx. 1 mbar. The difference in released pressure is then 0.35 mbar. Assuming that all desorbed gas was hydrogen, the mass would be 0.2 mg (in approx. 0.5 g sample). So the hydrogen absorption can be taken as negligible. This small observed absorption is most probably only to the surface layers of the sample since very small influence on structure-transition pressure was observed only in the data taken from the surface of the hydrogenated sample.

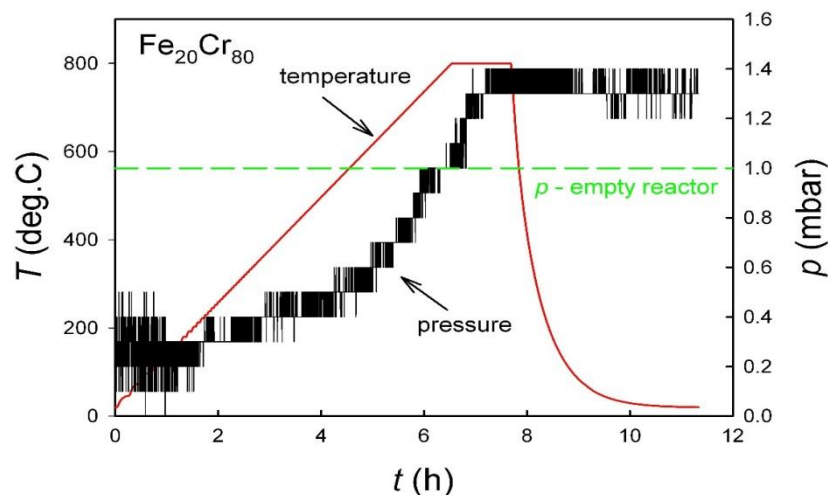


**Figure3.** The pressure and temperature variations as a function of time during the desorption experiment performed on Fe<sub>20</sub>Cr<sub>80</sub> in a closed volume.

#### 2.3 High-pressure X-ray diffraction

The XRD measurements, taken at ambient pressure confirmed the bcc structure type (Im-3m space group) of all samples. With increasing pressure, the crystal-structure transition from bcc to hcp structure type (P6<sub>3</sub>/mmc space group) is observed (fig. 4). The pressure in which the transition occurs was found to increase with increasing the Cr-concentration in the sample (from 13 GPa in Fe<sub>90</sub>Cr<sub>10</sub> to 18 GPa in Fe<sub>70</sub>Cr<sub>30</sub>— fig. 5 and

29.8 in Fe<sub>53</sub>Cr<sub>47</sub>). For the Cr-concentrations higher than 47 % we did not see any traces of the phase transition (fig. 6), probably because the pressure used (35 GPa) was not high enough to induce the structure transition in the alloys. The XRD pattern taken after the pressure was released shows that the crystal-structure transition is actually reversible. The symmetry of the crystal structure is restored. The Rietveld refinement of the data confirmed the same lattice parameter at ambient pressure and after releasing the applied external pressure.

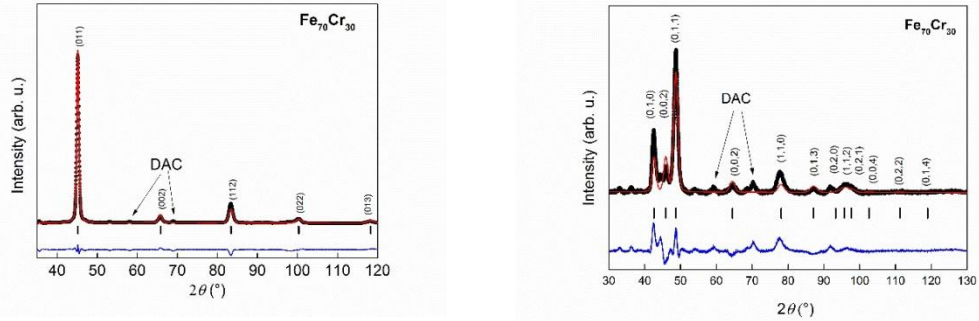


**Figure 4.** XRD patterns of Fe<sub>70</sub>Cr<sub>30</sub> at 6.9 GPa – left (bcc structure) and at 32.2 GPa – right (hcp structure). Red line – refined Rietveld profile, blue line – difference profile, vertical tick marks – Bragg position.

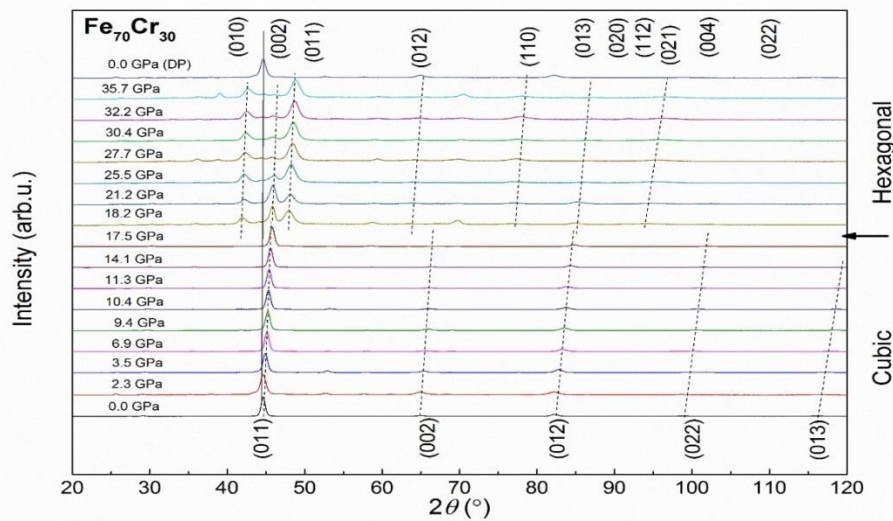


**Figure 5.** Pressure dependence of the XRD pattern of Fe<sub>70</sub>Cr<sub>30</sub>. The (DP) denotes the pattern taken after releasing the external pressure. The arrow denotes the phase transition. Solid line represents the reflection position at ambient pressure, the decrease of the lattice parameters is indicated by the tilted dotted lines.

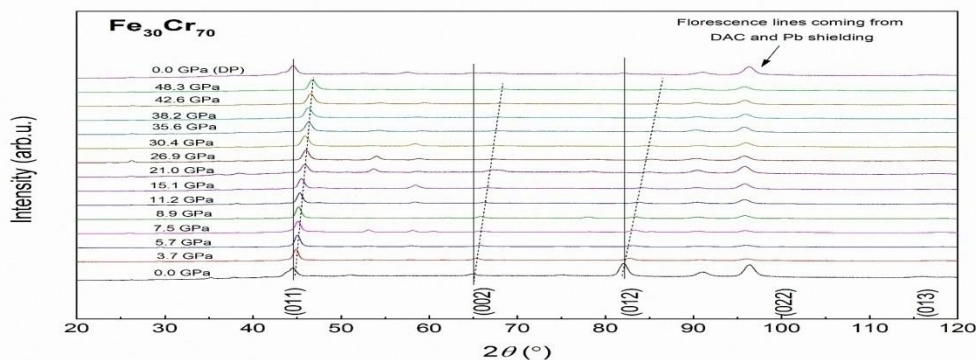


**Figure 6.** Pressure dependence of the XRD patterns of Fe<sub>30</sub>Cr<sub>70</sub>. The (DP) denotes the pattern taken after releasing the external pressure. Solid lines are reflection position at ambient pressure, the decrease of the lattice parameter is indicated by the tilted dotted lines.

Putting all the available data together we were able to establish a pressure-concentration phase diagram (fig. 7) of the Fe-Cr alloys showing how the crystal structure is changing with increasing Cr-concentration under applied pressure.

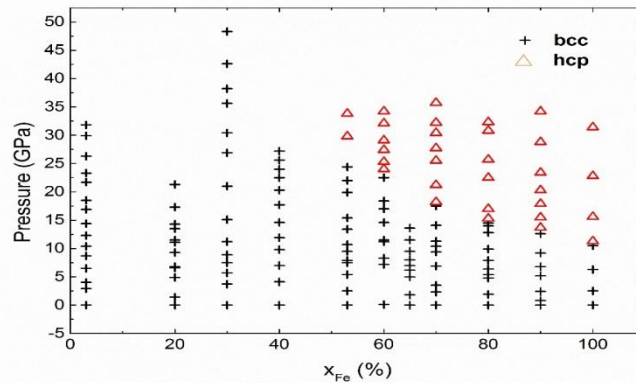


**Figure 7.** Phase diagram of Fe-Cr alloys showing the crystal structure as a function of pressure and composition. The “plus sign” denotes the bcc structure. The triangles denote the pressure-induced hcp phase.

### 2.4 High-pressure neutron diffraction

The neutron diffraction experiment shows some differences compared to the results of the XRD measurements. The transitions observed by the neutron diffraction occur in slightly higher applied pressures. Contrary to the XRD experiment, the pressure needed to induce the transition from bcc to hcp structure in Fe<sub>80</sub>Cr<sub>20</sub> is 3 GPa higher. The reason might be the absence of the pressure media in the pressure cell in the case of the neutron diffraction. The maximum pressure in the pressure cell used for neutron diffraction was limited by ~ 27 GPa. The difference in the transition-pressure between XRD and ND, and the limitation of the pressure cell did not allow us to see the transition for Fe<sub>60</sub>Cr<sub>40</sub> and higher Cr concentrations (24 GPa for XRD [14]) by neutron diffraction.

Figure 8 shows the comparison between the pressure dependence of the crystal structure of Fe<sub>80</sub>Cr<sub>20</sub> and its hydride. The transition was observed both in the parent compound and the hydride in approximately the same pressure. It is not surprising as the desorption experiment showed that the surface hydrogen absorption is only negligible.

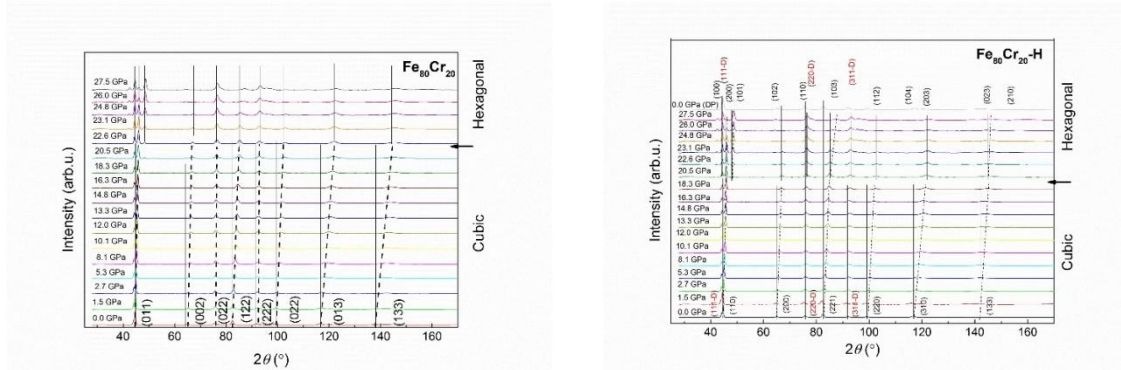


**Figure 8.** The pressure dependence of the neutron-diffraction pattern of Fe<sub>80</sub>Cr<sub>20</sub> (left) and Fe<sub>80</sub>Cr<sub>20</sub>-H (right). The arrow denotes the pressure of the crystal-structure transition.

The Rietveld refinement of the XRD and ND patterns gave us the change in the unit cell parameter as function of pressure, subsequently also the volume changes (figs. 9, 10). The pressure dependence of the volume was then fitted to the Vinet equation of state (1) [15]

$$p(V) = 3B_0 \left( \frac{V}{V_0} \right)^{-2/3} \left( 1 - \left( \frac{V}{V_0} \right)^{1/3} \right) \exp \left( \frac{3}{2} (B_0' - 1) \left( 1 - \left( \frac{V}{V_0} \right)^{1/3} \right) \right) \quad (1)$$

Figures 9 and 10 show the fits and the parameters of the Vinet equation used for selected samples. The results of the fitting provided us with the  $B_0$  and  $B_0'$  which represent the compressibility of the samples (fig. 11).

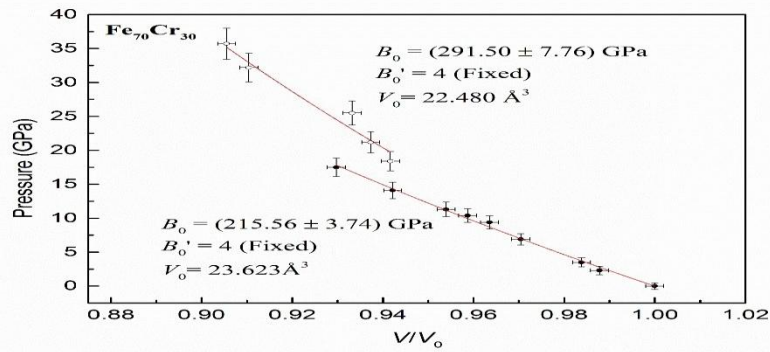


**Figure 9.** The pressure dependence of the volume of Fe<sub>70</sub>Cr<sub>30</sub>. The red curves represent the fits to the Vinet equation of state both for the cubic and hexagonal phase.

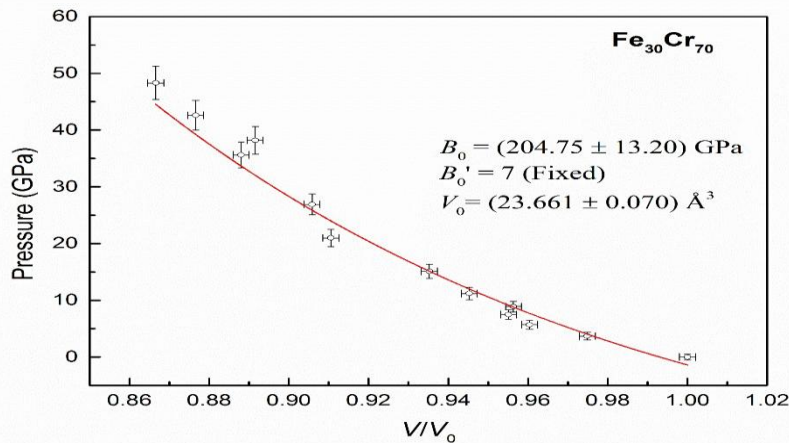


**Figure 10.** The pressure dependence of the volume of Fe<sub>30</sub>Cr<sub>70</sub>. The red curve represents the fit to the Vinet equation of state.

Comparing the parameters of Vinet equation for Fe<sub>80</sub>Cr<sub>20</sub> and its hydride (Tab. 1) we can see that the values are slightly different due to the surface hydrogen absorption (but still within the experimental error).

**Table 1.** Comparison between B<sub>0</sub> and V<sub>0</sub> for Fe<sub>80</sub>Cr<sub>20</sub> and its hydride obtained from neutron and X-Ray diffraction experiments.

|     | Fe <sub>80</sub> Cr <sub>20</sub> |                                  | Fe <sub>80</sub> Cr <sub>20</sub> -H |                                  |
|-----|-----------------------------------|----------------------------------|--------------------------------------|----------------------------------|
|     | B <sub>0</sub> (GPa)              | V <sub>0</sub> (Å <sup>3</sup> ) | B <sub>0</sub> (GPa)                 | V <sub>0</sub> (Å <sup>3</sup> ) |
| XRD | 225.50 ± 9.44                     | 23.556 ± 0.035                   | -                                    | -                                |
| ND  | 225.87 ± 1.96                     | 23.483 ± 0.005                   | 204.10 ± 23.36                       | 23.468 ± 0.005                   |

The concentration dependence of the values of the Bulk modulus (fig. 11) follows the same trend as the electrical resistance measured by A. Gorbunov et al. [16]. The Bulk modulus of elemental Iron was shown to be (167 ± 2) GPa [17]. It is increasing with increasing Cr concentration up to approx. 30 % Cr. Then it starts to decrease again followed by another increase and subsequent decrease represented by a double-peak dependence on Cr concentration (fig. 11). Finally the Bulk modulus of elemental Cr, 160 GPa, is similar to the one of Fe [18].

The possible reason for the double-peak dependence was discussed in [16]. It was stated that the maxima in resistance in the regions 30 < x < 38 at. % Cr and 55 < x < 70 at. % Cr occur most probably due to the phase mixtures present in these concentration ranges (fig. 1 in [16]) which introduce additional scattering for the conduction electrons at the phase boundaries. At nearly equiatomic compositions, single phase alloys form. This partial ordering results in a minimum of resistance. Similar reason (phase and grain boundaries) can be considered also for hardening of the lattice (concentration dependence of B<sub>0</sub>).

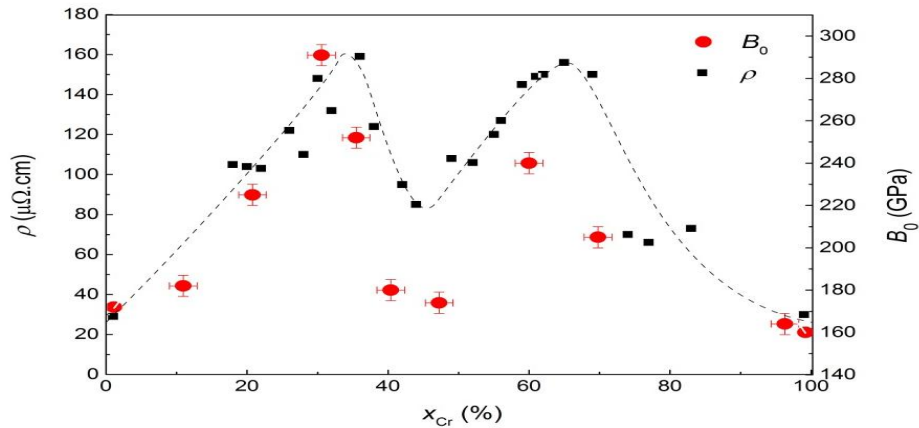


**Figure 11.** Concentration dependence of the electrical resistence (black squares) [16] and the bulk modulus  $B_0$  for  $\text{Fe}_{100-x}\text{Cr}_x$ . The dashed line is a guide for eye.

#### IV. Conclusions

All samples from the  $\text{Fe}_{100-x}\text{Cr}_x$  series were found to be crystallizing within the bcc phase without any traces of the sigma phase or oxide. With increasing pressure the crystal structure reversibly changes from bcc to hcp structure type at least up to 47 at.% Cr. For higher concentrations, the pressure used (35 GPa) was not high enough to induce the structure transition in the alloys. With increasing Cr-concentration the structure transition is shifted to higher pressures. The Bulk modulus is highly dependent on Cr-concentration. It is characterized by a double-peak dependence on Cr concentration.

#### References

- [1]. M.S. Lucas, M. Kresch, R. Stevens, and B. Fultz, Phonon partial densities of states and entropies of Fe and Cr in bcc Fe-Cr from inelastic neutron scattering, *Phys. Rev. B* 77 (2008)184303.
- [2]. M.S. Lucas, A. Papandrew, and B. Fultz, Partial phonon densities of states of  $^{57}\text{Fe}$  in Fe-Cr: Analysis by a local-order cluster expansion, *Phys. Rev. B* 75 (2007) 054307.
- [3]. R.L. Kluehand D.R. Harries, High-Chromium Ferritic and Martensitic steels for Nuclear Application, Library of Congress Cataloguing in Publication data by American Society for Testing and Materials (ASTM) (2001).
- [4]. A. Kohyama, A. Hishinuma, D.S. Gelles, R.L. Klueh, W. Dietz, K. Ehrlich, Low-activation ferritic and martensitic steels for fusion application, *J. Nucl. Mater.* 233-237 (1996) 138-147.
- [5]. O. Kubaschewski, Phase Diagrams of Binary Fe-Based Systems, Springer Verlag, Berlin-Heidelberg and Verlag Stahleisen mbH, Dusseldorf (1982).
- [6]. R.M. Fisher, E.J. Dulis, and K.G. Carroll, Identification of the precipitate accompanying 885 F embrittlement in Cr steels, *Trans. AIME* 197 (1953) 690-695.
- [7]. R.O. Williams, and H.W. Paxton, The Nature of Aging of Binary Iron-Chromium Alloys Around 500 °C, *J. Iron Steel Inst.* 185 (1957) 358-374.
- [8]. D. Bancroft, E. L. Peterson, and S. Minshall, Polymorphism of Iron as High Pressure, *J. Appl. Phys.* 27 (1956) 291-298.
- [9]. E. Sterer, M.P. Pasternak, R.D. Taylor, A multipurpose miniature diamond anvil cell, *Rev. Sci. Instrum.* 61 (1990) 1117-1119.
- [10]. R.A. Forman, G.J. Piermarini, J.D. Barnett, S. Block, Pressure measurement made by the utilization of ruby sharp-line luminescence, *Science* 176 (1972) 284-285.
- [11]. J. Rodriguez-Carvajal, Recent developments of the program FULLPROF, *Comm. Powder Diffr. IUCr Newsl.* 26 (2001) 12–19.
- [12]. A.S. Tremsin, J.B. McPhate, J.V. Vallerga, O.H.W. Siegmund, W.B. Feller, H.Z. Bilheux, J.J. Molaison, C.A. Tulk, L. Crow, R.G. Cooper, D. Penumadu, Transmission Bragg edge spectroscopy measurements at ORNL Spallation Neutron Source, *J. of Physics:Conference Series* 251 (2010) 12069.
- [13]. H.M. Rietveld, A Profile Refinement Method for Nuclear and Magnetic Structures, *J. Appl. Crystallogr.* 2 (1969) 65-71.
- [14]. O. Rivin, A. Broide, S. Maskova, M.S. Lucas, A. Hen, I. Orion, S. Salhov, M. Shandalov, A. Moreira Dos Santos, J. Molaison, Z. Chen and I. Halevy, High pressure neutron powder diffraction study of  $\text{Fe}_{1-x}\text{Cr}_x$  with and without Hydrogen exposure, *Hyperfine interaction* 231 (2015) 29-36.
- [15]. P. Vinet, J. Ferrante, J.H. Rose, J.R. Smith, Compressibility of solids, *J. Geophys. Res.* 92 (1987) 9319-9325.
- [16]. A. Gorbunov, A. A. Levin, D. C. Meyer, L. Bischoff, D. Eckert, B. Kohler, M. Mertig, T. Weißbach, E. Wieser, and W. Pompe, Correlation of structural and physical properties of metastable Fe-Cr phases, *Cryst. Res. Technol.* 40, No. ½ (2005) 106 – 113.
- [17]. S. A. Kim, W. L. Johnson, Elastic constants and internal friction of martensitic steel, ferritic-pearlitic steel, and  $\alpha$  iron, *Materials Science and Engineering A* 452–453 (2007) 633–639.
- [18]. P. W. Bridgman, Compressibilities and Pressure Coefficients of Resistance of Elements, Compounds, and Alloys, Many of Them Anomalous, *Proc. Amer. Acad. Arts Sci.* 68 (1933) 27-93.